CHAPTER IV
PREPARATION AND CHARACTEIZATION OF POLY(VINYLIDENE FLUORIDE) / BACTERIAL CELLULOSE NANOCONPOSITE FILMS

4.1 Abstract

The bio-based piezoelectric nanocomposite films were prepared from the blends of poly(vinylidene fluoride) (PVDF) and bacterial cellulose (BC) at various weight compositions (PVDF/BC: 100/0, 97.5/2.5, 95/5, 90/10, 80/20, and 60/40). The nanocomposite films were suscessfully fabricated via two steps: solvent casting follwed by hot-pressing technique. The intermolercular interaction between PVDF and BC had influenced to crystalline phase behavior, thermal, mechanical and dielectric properties of the film. The properties of this blend system was studied in the feature of using as piezoelectric touch sensor. All blend films were mainly formed in polar β-polymeric crystalline phase. The storage modulus of the blend flims were higher than neat PVDF as increasing BC contents up to 10 wt%. In addition, 10 wt% loading of BC offer the superior dielectric properties over the neat PVDF, the dielectric constant of $PVDF_{90}BC_{10}$ was increased to 6.92, 4.85 and 4.32 at frequency of 10 MHz, 100 MHz and 1 GHz, respectively.

4.2 Introduction

The direct piezoelectric effect of materials is the basis for mechanical sensor applications since an applied mechanical stimuli (force, pressure and vibrations) change the polarization of materials resulting in electrical charge or dielectric displacement (Harrison and Ounaies, 2001). Piezoelctric materials were introduced as touch sensor to overcome limitations of common touch technology by combine the benefits of both capacitive and resistive touch sensor. The piezoelectric materials can response to both of charged and uncharged objects like resistive screen and has high sensitivity like capacitive screen. Morover, it has ability to harvest

mechanical energy to power itself: operated without external battery in the near future.

Piezoelectricity of semi-crystalline polymers have been explored since they present a number of advantages, in term of light weight, flexibility, cheap and ease of process compared to the conventional piezoelectric materials (Harrison, 2001; Choi, 2009; Uehara, 2011). A ferroelectric polymer like poly(vinylidene fluoride) (PVDF) exhibit highest piezoelectric behavior (Gregorio, 1999; Salimi, 2003) than other polar semi-crystalline polymer. PVDF has an absence of asymmetric crystal of its β polymeric crystalline phase with molecules take all trans conformation resulting in highest dielectric and piezoelectric properties.

Due to the demand of using synthetic polymer is greater every year, environmental problems (Ratanakamnuan, 2012) such as exhausting petroleum source, waste management and biodegrability become a major role in polymeric research and indutry. The bio-based polymer composites, combination of synthetic polymer and bio-materials, have drawn scientific interest to develop the composites in order to reach the superior properties of each component.

Bacterial cellulose (BC) is a biopolymer with nano-ribbon-shaped like which consisting of anhydroglucose units, bonded together via β-1,4-glycosidic linkage as same as plant cellulose. The hydroxyl group of BC can provide partially miscible with polymer containing functional group, e.g. polyurethane (Seydibeyoglu, 2007), polyethylene oxide (Park, 2007), poly(vinyl pyrrolidone) (Rao, 2002) and poly(vinyl alcohol) (Tang, 2008). The incorporation of BC to polymer matrix offers more environmental friendly, thermal stability, dimensional stability, and higher mechanical strength.

The aims of this study were to prepared the PVDF/BC blend films to extending the ability of bio-piezoelectric nanocomposite as a high-performing materials. The β crystalline phase of the PVDF/BC blends were investigated to confirm piezoelectric behavior compare to neat PVDF. The nano-fiber create higher interfacial adhesion between high electro-negativity atoms (fluorine and oxygen) which their dielectric, morphological, thermal and mechanical properties of the films were strongly discussed.

4.3 Experimental Procedures

4.3.1 Materials

Nata de coco was purchased from local food factory as a food grade. PVDF (J100) was supplied by Asambly Chemicals Company. N,N-dimethylformamide (DMF) and sodium hydroxide (NaOH) were purchased from RCI Labscan Co.,Ltd. and Merck Ltd., respectively.

4.3.2 Extraction and Purification of Bacterial Cellulose

Bacterial cellulose (BC) was extracted from nata de coco product. The nata de coco gel were firstly rinsed with distilled water and blended using a laboratory blender. Then, nata de coco gel was treated with 0.1 M NaOH at 80°C for 1 hour to remove any remaining microorganisms, medium component and soluble polysaccharides. The purified bacterial cellulose will be then thoroughly washed with distilled water until reached the neutral pH.

4.3.3 Fabrication of Nanocomposite Films

The nanocomposite films were firstly prepared by solvent casting technique. DMF was used as solvent to dissolve PVDF at 60°C and stirred until the homogeneous solution was obtained. Then, BC and PVDF were mixed together at the desired weigh ratio of PVDF/BC (100/0, 97.5/2.5, 95/5, 90/10, 80/20, and 60/40). The mixtures were stirred at 60°C for 30 minutes to allow good distribution then poured on Petri dish glass. After the solvent was vaporized in an oven at 80°C for 48 hours in order to remove all remaining solvent, the BC/PVDF films were obtained with void trapped inside from solvent evaporated. Then, hot-pressed technique was used to make a dense film. The casted films were heated at 180°C for 20 minutes without pressure to make polymer completely in molten state, followed by 10 tons of pressure for 5 minutes. Finally, the films were about 0.5 mm in thickness.

4.3.4 Characterizations

The morphology and dispersion of BC of cross-sectional samples were observed through a field emission scanning electron microscopy (Hitachi, S-4800). Fourier transform infrared spectroscopy (Nicolet, NEXUS 640) was used to determine crystalline phases of the films. The dielectric constant and dissipation factor were measured using a Network Analyzer (Agilent, E4991A). Dynamic

mechanical analysis was performed in tension mode using a GABO, EPLEXOR 100N at a constant frequency of 1 Hz to determine dynamic T_g and mechanical relaxation temperature of the blend films . Ferroelectric measurement was performed using RT66A at room temperature to observed P-E hysteresis loops of samples.

4.4 Results and Discussion

4.4.1 Bacterial Cellulose Characterization

4.4.1.1 Crystallinity of BC

The X-Ray diffraction pattern of bacterial cellulose sheet prepared from nata de coco was displayed in Figure 4.1. The result shows three main diffraction signals occurring in the region of 10-30° at 2θ approximately 14.5°, 16.9° and 22.5° assigned to diffraction planes 110, 110 and 200, respectively. This result was strongly associated with crystal lattice of cellulose I (Adnan, 2012; Czaja, 2004) which consisted of two different crystal structures, a one-chain triclinic structure I_α and two-chains monoclinic structure I_β . The calculated crystallinity index (CrI) and crystalline size (equations 3.2 and 3.3) at diffracted rays are shown in Table 4.1. The BC that purified from nata de coco had smaller crystallite size at 200 diffraction plane than BC in static culture.

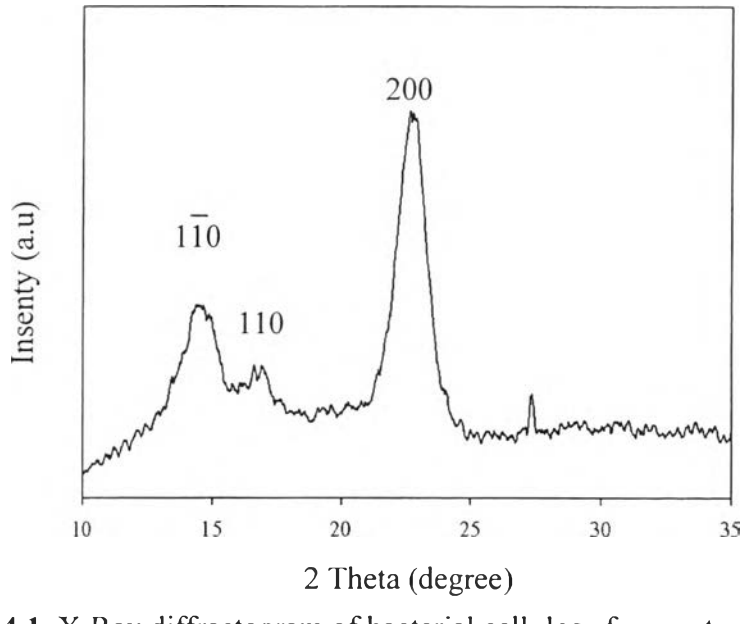

Figure 4.1 X-Ray diffractogram of bacterial cellulose from nata de coco.

Table 4.1 Crystallinity Index and crystallite size of bacterial cellulose

Samples	CrI	Crystalline size (nm)		
		110	110	200
BC	-	38.1	42.0	29.2
BC-nata de coco	77.6	-	-	16.9

4.4.1.2 Morphological Observation of BC

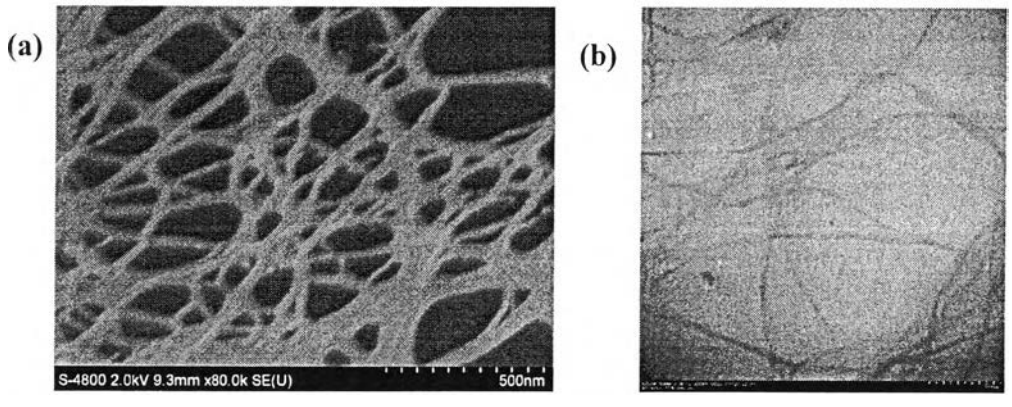

Figure 4.2 SEM image of dried BC film (a) and TEM image of purified BC (b).

The dried bacterial cellulose sheet was prepared via diffusion method, all of liquid state diffuse though PTFE membrane to decreased drying rate and prevented agglomeration of network fibers. The SEM and TEM were employed to detemine the shape and diameter of the purified bacterial cellulose as shown in Figure 4.2 (a) and (b), respectively. These images show BC exhibited nano-porous network structure as ribbon-shaped fibrils with diameter about 30-50 nm which smaller than one-tenth of the visible light wavelength (400-800 nm). The results confirmed that the obtained BC was in nano-scale (one diameter less than 100 nm) via diffusion technique. The network fiber exhibited high surface area which yield to high possibility of hydroxyl group on BC surface interact with polar polymer matrix or polar filler via both of physical and chemical interactions. In addition, nano-cellulose composites exhibit higher optical and mechanical properties compare to micro-crystalline cellulose (MCC). Because the BC nanocomposite has less air interstices yield to lower loss of incident light (Khalil, 2012).

4.4.2 PVDF/ BC Blends Characterization

4.4.2.1 Morphologies of The Blends

The bio-based polymer blends of PVDF and BC were obtained from two steps of solution casting and compression technique. The SEM micrograph of purified bacterial cellulose (Figure 4.2) demonstrated BC showed approximate diameter around 30-50 nm which can be called nano-material. To achieve superior properties of combining nano-network fiber, the fabrication process become essential step to prevent BC in nano-scales agglomerate into macro-scales. Because three hydroxyl groups per repeating unit of BC exhibited strong hydrogen bonding between the fibrils. The scanning electron microscopy (SEM) were used to confirmed that this research was successfully prepared the nanocomposite films.

The Figures 4.3 (a) and (b) show a cross-sectional SEM images of casted film of 10 wt% network fibers loading at a magnification of 1k and 10k, respectively. At 1k, the evaporation of DMF generated voids inside the nanocomposite film. To observe the diameter of the fiber after incorporated with PVDF, the magnification was increased to 10k. The result (Figure 4.3 (b)) shows that the diameter of BC was approximately about 40-50 nm as a heterogeneous fiber dispersed in PVDF matrix. However, containing bubbles in the films cause opaque appearance, electrically defects and poor mechanical properties. Thus, the compression technique was introduced to make dense films. PVDF molten moved to full-filled all of fiber spacing under high pressure of 10 tons. The cross-sectional of compressed films at various BC contents were shown in Figure 4.4. The compressed films had no air interstices resulting in smooth surface, higher percent light transmittance, lower dielectric loss and higher dielectric breakdown strength (Sodsong, 2008). As increasing the content of BC (Marcovich, 2006), the appearance of fracture surface become rougher due to higher dissipation energy during fractured. BC can act as bio-filler (rigid filler), which the different in rigidity created difference cracking pathways. Except, $PVDF_{80}BC_{20}$ film still containing voids since the amount of PVDF molten was not enough to penetrate to all spacing between network fiber and polymer matrix.

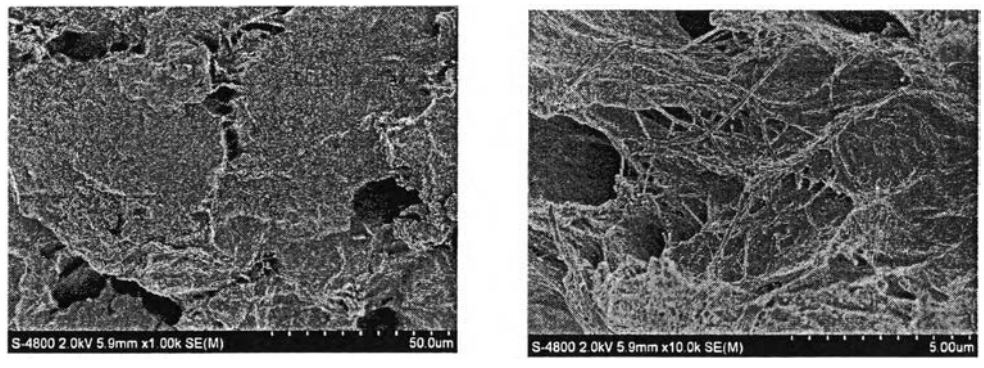

Figure 4.3 SEM images of casted $PVDF_{90}BC_{10}$ films at (a) 1k and (b) 10k.

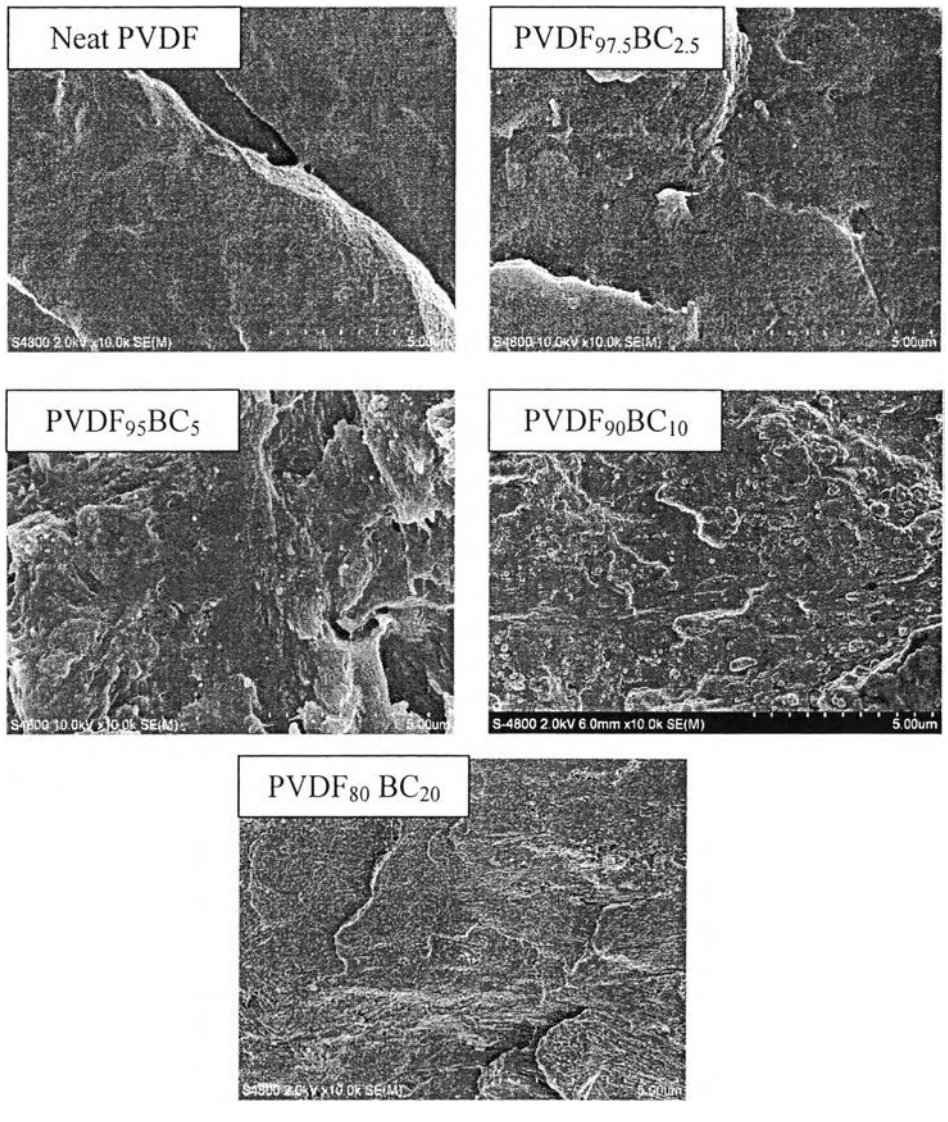

Figure 4.4 SEM images of PVDF/BC blends at different weight compositions.

4.4.3 Crystalline Phase Behavior

The chemical formula of PVDF is $-CH_2-CF_2-$ which exists of 4 molecular conformations (α, β, δ, and γ), depending on trans and gauche isomers taken between fluorine atoms and oxygen atoms to the polymer backbone. The β-phase (all-Trans) is only one of these conformations, exhibit piezoelectricity due to it shows the strongest dipole-moment following Debye-model. To understand phase behavior, the crystal structure of the compressed film of the neat PVDF and PVDF/BC blends were identified and discussed using FTIR and XRD techniques.

From the infrared spectra as shown in Figure 4.5, the absorption bands characteristic of neat PVDF and composites demonstrated that they consisted of two common polymorphs referring to α and β phases. The molecules in α phase show vibration band at 530 cm^{-1}(CF_2 bending), 612 cm^{-1} and 763 cm^{-1} (CF_2 bending and skeletal bending) and 795 cm^{-1} (CF_2 rocking). The formation of β-phase, all-trans planar zigzag conformations, was observed by a presence of specific absorption bands at 510 cm^{-1} (CF_2 bending) and 840 cm^{-1} (CH_2 rocking).

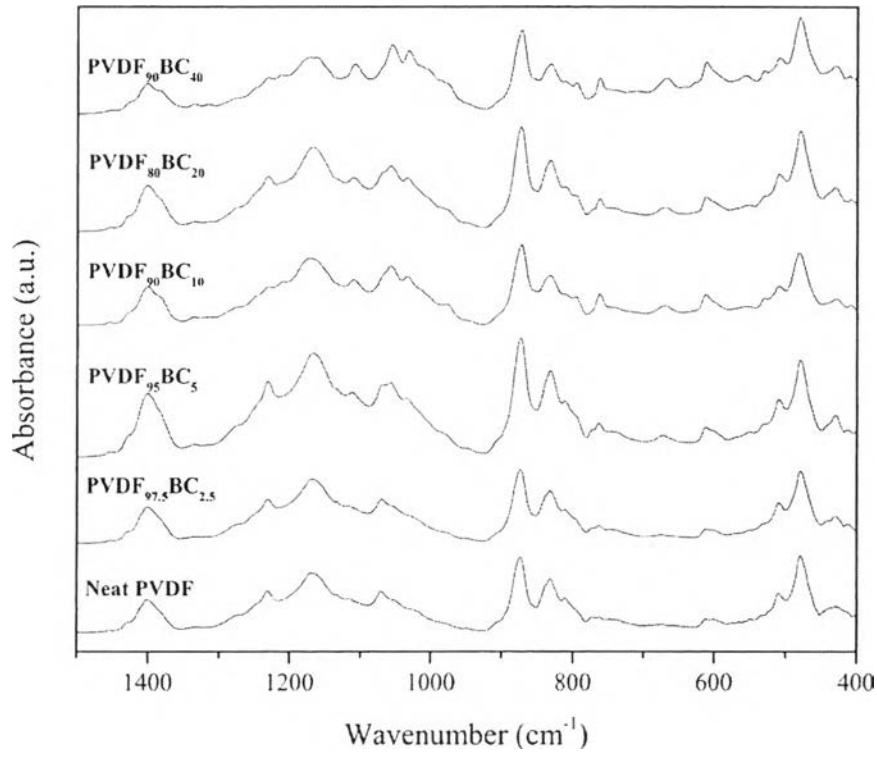

Figure 4.5 FTIR spectra of compressed neat PVDF and PVDF/BC blend films.

Table 4.2 β-phase contents, F(β) (%) of PVDF and PVDF/BC blends

PVDF/BC	β-phase contents, F(β) (%)
100/0	71.42
97.5/2.5	63.11
95/5	65.02
90/10	63.25
80/20	61.44
60/40	51.43

Due to the β crystalline phase dependent the pyro- and piezoelectricity of the films, the fraction of β phase, F(β), of the films were calculated from the intensity of absorption bands by Beer-Lambert law (equation 3.1). The F(β) of neat PVDF and PVDF/BC blends are shown in the Table 4.2. The maximum β phase content (71.42%) was obtained from neat PVDF. As increasing the amount of BC, the absorption bands in β phase decreased in intensity due to the network fiber disrupted the ability to form β crystalline phase of PVDF matrix. The previous researches were found that F(β) could be improved by adding molecules containing fluorine, oxygen or nitrogen atoms, to form H-bond interaction with F-atoms of PVDF and create β polymeric form. In contrast, BC is a ultra-fine network fiber which owygen atoms in ether linkages and hydroxyl groups have random direction. Thus, the formation of crystalline regions in PVDF/BC blends resulted in higher amount of α phase crystals, the simplest conformation (TGTG'), compared to neat PVDF films.

Figure 4.6 shows XRD patterns of crystalline state of compressed PVDF and PVDF/BC blends at 2.5, 10, 20 and 40 wt% of BC loading. The result demonstrated that the crystal polymorph of PVDF sheet reflected into β and α phases which their unit cells are orthrorhombic and monoclinic type, respectively. The peaks of β-crystalline phase exhibited 2θ at 20.4°, 36.7° and 40°. Nevertheless, diffraction peaks at 18.6° and 27° are assigned to α-crystalline phase (Jiang *et al.*, 2004). Although, the XRD patterns of $PVDF_{97.5}BC_{2.5}$ film was apparently similar to the neat PVDF. The absence of small peak of α phase at 27° yeild to $PVDF_{97.5}BC_{2.5}$ showed

higher β/α ratio than neat PVDF. The intensity of β and α phase of PVDF are decrease when blending with large content of BC due to the network fiber interrupting the crystal formation of polymer matrix. In addition, the small peak at around 22.6° was cleary obsearved corresponding to 200 diffractions plane of BC.

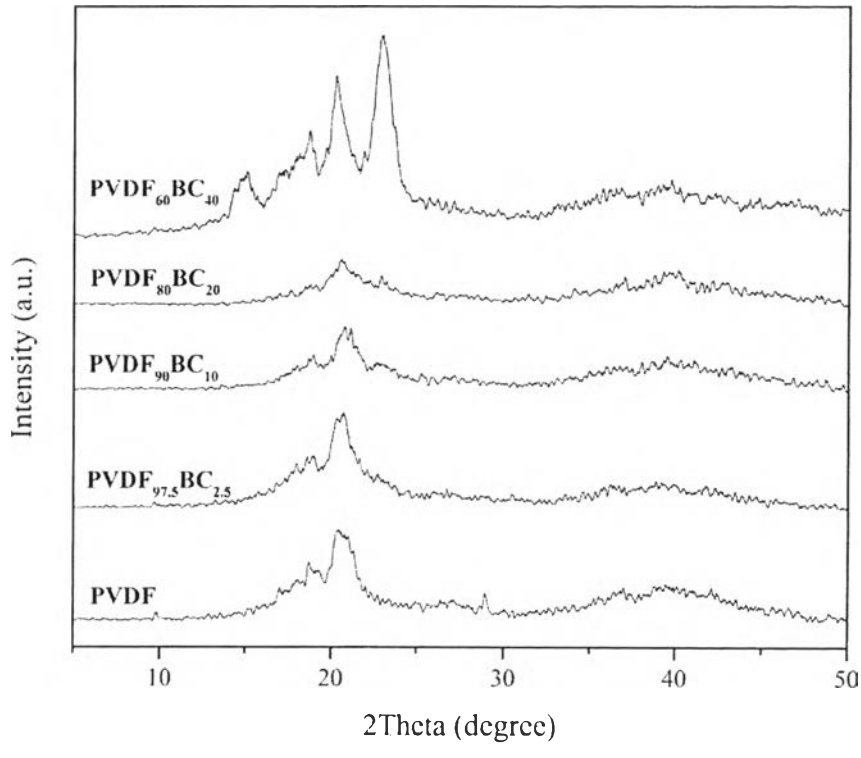

Figure 4.6 X-ray diffraction patterns of PVDF and PVDF/BC blends films.

4.4.4 Thermal Properties

The glass transition (T_g) and melting temperature (T_m) of neat PVDF and PVDF/BC blends films were characterized by DSC measurement at a constant heating rate of 10 °C/min. Figure 4.7 shows the second-heating DSC thermograms of PVDF and PVDF/BC blends with different contents of BC. The DSC parameters are shown in Table 4.3. During the second heating cycle, two transition regions were observed at temperature about -40 °C and 160 °C which corresponding to T_g and T_m, respectively. The amorphous regions of neat PVDF exhibited T_g at about -38.96 °C. In comparison with neat PVDF, the nanocomposite with the addition of BC (Li,

2010), result in a slightly decreased in T_g refer to BC did not hindered molercular motion of PVDF from glassy state to rubberry state. The slightly increasing in T_m arised from, the small intermolecular interaction between vinylidine fluoride and anhydroglucose units, result in increased T_m of nanocomposites about 1-2 °C compare to neat PVDF.

In this blends system, only PVDF part can be melted while BC cannot melt: degradation temperature (T_d) of cellulose is higher than T_m. Thus, the addition of BC decreased the enthalpy changes for melting (ΔH_m) refer to less amount of PVDF matrix that absorbed the enthalpy to melt. Thus, the percentage crystallinity (X_c) have to be calculated comparing to PVDF compositions of each sample (as Equation 3.4). The X_c results implied that X_c decreased with increased BC contents up to 10 wt%, which signified that the nanofiber disrupting the movement of PVDF molecular chain to form a crystalline region. In contrast, at higher amount of BC, the $PVDF_{80}BC_{20}$ exhibited higher X_c because each polymer phases were partially separated and agglomerated, as observed from SEM micrographs, to form higher crystalline part.

Table 4.3 DSC parameters of PVDF and PVDF/BC blend films

Sample	ΔH_m(J/g)	T_g (°C)	T_m (°C)	X_c (%)
PVDF	41.65	-38.96	161.51	40.56
$PVDF_{97.5}BC_{2.5}$	40.09	-40.25	160.88	40.04
$PVDF_{95}BC_5$	37.38	-39.95	161.78	38.31
$PVDF_{90}BC_{10}$	33.10	-40.02	162.01	35.8
$PVDF_{80}BC_{20}$	33.87	-39.18	162.64	41.22
$PVDF_{60}BC_{40}$	29.03	-38.57	159.88	47.55

*Heat of fusion value for 100% crystalline PVDF, ΔH_0= 102.7 J/g

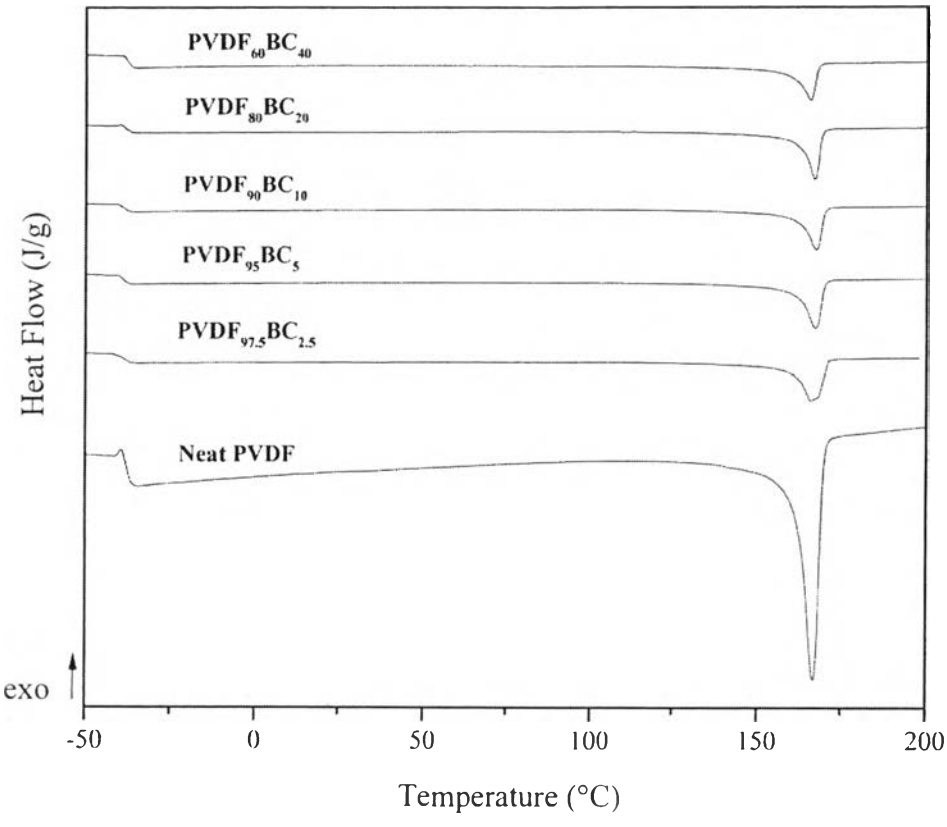

Figure 4.7 DSC second-heating curves of PVDF and PVDF/BC blends films.

TGA experiments have been carried out to identify the degradation temperature and weight loss of materials. The samples were heated from 30 °C to 900 °C in nitrogen atmosphere at a heating rate of 10 °C/min. Figure 4.8 illustrates TGA curves as a plot of weight loss versus temperature of compressed PVDF and PVDF/BC nanocomposite films. The onset and maximum degradation temperature (T_d,onset and T_d,max) are summarized in Table 4.4. The neat PVDF showed single weight loss at temperature around 421.62 °C, whereas PVDF/BC nanocomposite showed two steps of weight loss. The first step occurred at 310-345 °C refer to the decomposition temperature of BC. The second composition is attributed to PVDF region decomposing at temperature ranging from 455-485 °C depend on BC composition. The thermal stability of PVDF in the blends were significantly enhanced with increasing fiber content. Blending 40 wt% of BC resulted in an improved thermal stability of PVDF by 45 °C higher than that of neat PVDF. This

shift is probably due to the increase in H-bonding interaction associated with an increasing BC content. Moreover, as solvent contaminated concern, TGA thermogram was used to confirmed no solvent trapped within materials which the thermograms had no step of weight loss from the solvent (boiling point of DMF is about 153 °C).

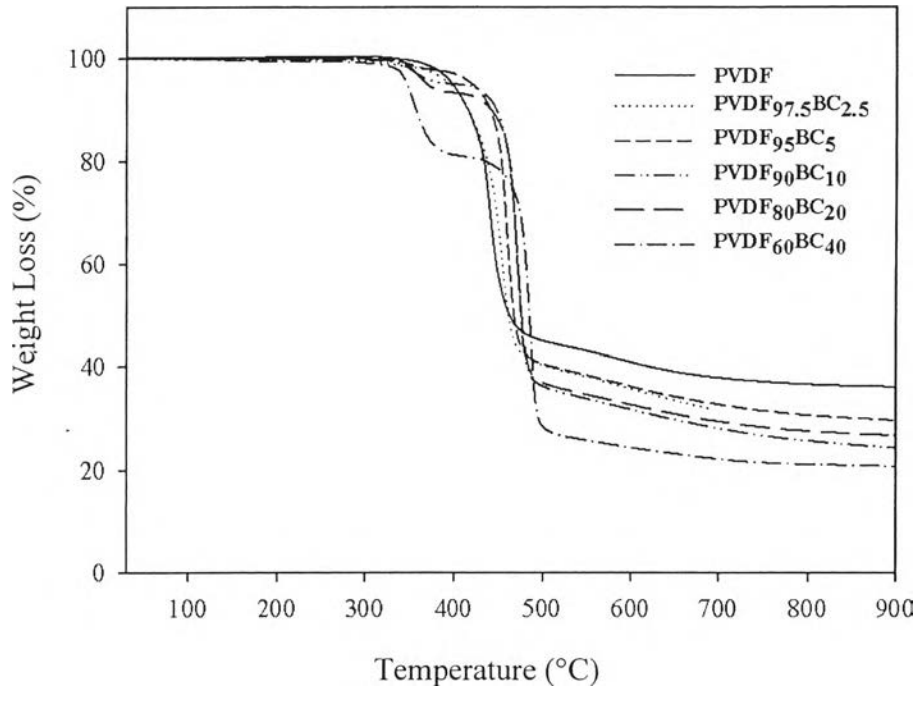

Figure 4.8 TG-DTA thermograms of PVDF and PVDF/BC blends films.

Table 4.4 TGA parameters of PVDF and PVDF/BC blend films

Sample	T_{d1} (onset)	T_{d2} (onset)	T_{d1} (max)	T_{d2} (max)
PVDF	-	421.62	-	439.76
$PVDF_{97.5}BC_{2.5}$	311.50	431.81	328.35	454.39
$PVDF_{95}BC_5$	324.98	447.46	349.70	460.22
$PVDF_{90}BC_{10}$	337.36	459.81	353.94	471.79
$PVDF_{80}BC_{20}$	344.85	459.43	361.64	471.27
$PVDF_{60}BC_{40}$	339.99	474.93	354.57	486.76

4.4.5 Dynamic Mechanical Properties

The thermal evaluations of storage modulus of casted and compressed samples were shown in Figure 4.9. The measurement were carried out over a range of temperature (-80°C to 150°C) at a constant frequency of 1 Hz. As results, the compressed film showed significant increase in storage modulus (E') more than casted film because of no void defect. The compressed film explored improving on mechanical properties at a given temperature.

Figure 4.10 shows the relation between dissipation factor (E''/E') and the temperature. Three relaxation regions were observed assigned to β, β', and α relaxation state. First relaxation is occurred at temperature about -40 °C which refer to dynamic glass transitions temperature (T_g) of material, called β relaxation, resulting from molecular movement in amorphous regions. The T_g of all compressed films shift to higher temperature due to pressure press cause molecule rearranged into better chain packing. Moreover, the sharp increase in dissipation factor of compressed films also observed at about 60 °C corresponding to the β' relaxation (Patro *et al.*, 2008). This weak relaxation arises from compressed-force makes polymer molecules in amorphous regions became folded. The third relaxation called α relaxation, which associated with segmental motion in crystalline regions, exhibited at around 150 °C which close to melting temperature of PVDF.

The thermodynamic response of compressed PVDF/BC blend films as a function of bacterial cellulose content are shown in Figure 4.11. In the presence of 20 wt% of BC, the storage modulus is higher than other blends about 1000 MPa throughout the temperature range from -80 °C to 150 °C. While the blend of 2.5 and 5 wt% BC show the almost similar storage modulus compared to neat PVDF. The patterns of dissipation factor vs. temperature of PVDF and its composite are quite the same, as shown in Figure 4.12. The relaxation regions of each blend also contributed into 3 transitions corresponding to β, β' and α transitions as same as neat PVDF. The relaxation temperature and storage modulus of compressed PVDF and nanocooposite films are summarized in Table 4.5. The β relaxation which is a first thermal transition in dissipation factor assigned to dynamic T_g. The dynamic T_g shifted towards to lower temperature from -38.4 to -40.6 °C (related to T_g from DSC data) with increasing fiber content. Because this observed T_g is associated with only PVDF

in amorphous regions. Thus, the composite that containing higher amount of BC required less energy to relax PVDF chains from glassy state to rubbery state.

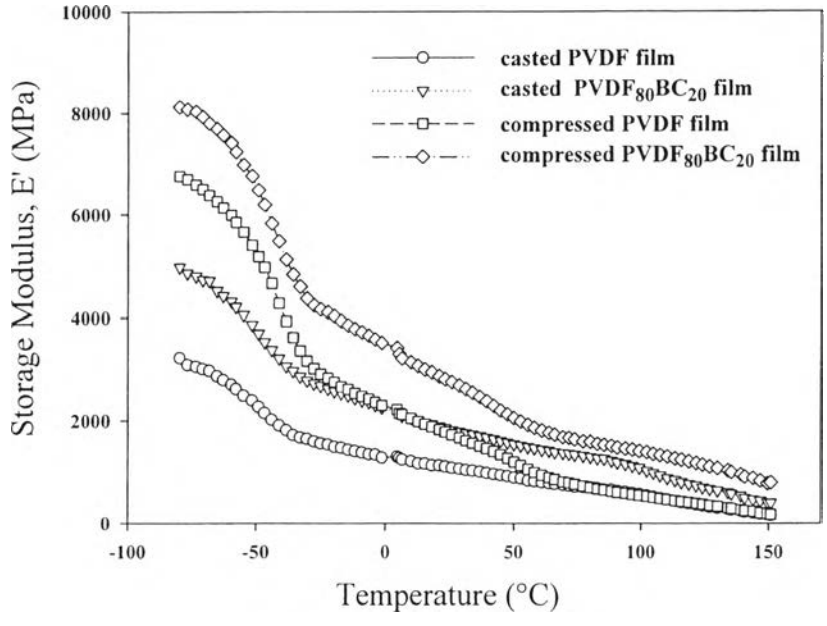

Figure 4.9 Storage tensile modulus, E' vs. temperature of PVDF and $PVDF_{80}BC_{20}$ via solvent-cast and compression technique.

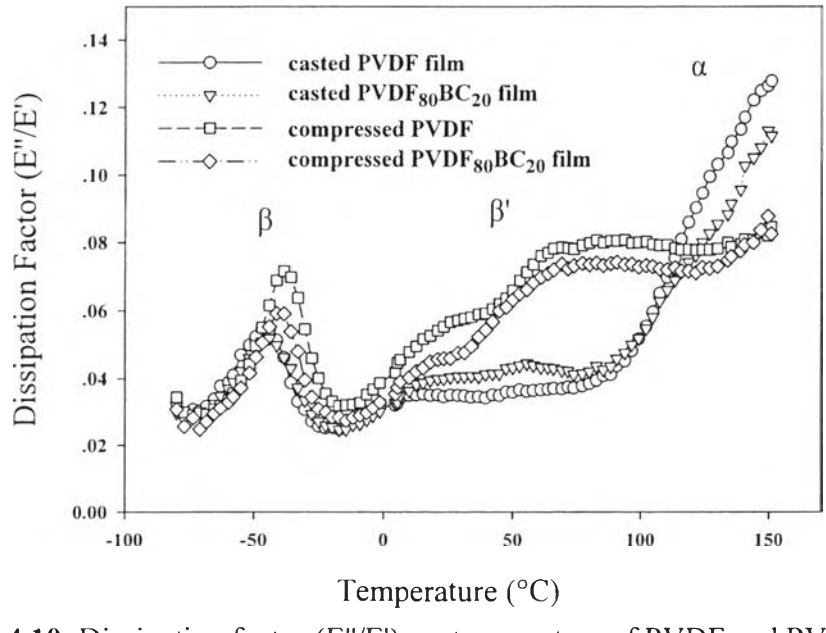

Figure 4.10 Dissipation factor (E''/E') vs. temperature of PVDF and $PVDF_{80}BC_{20}$ via solvent-cast and compression technique.

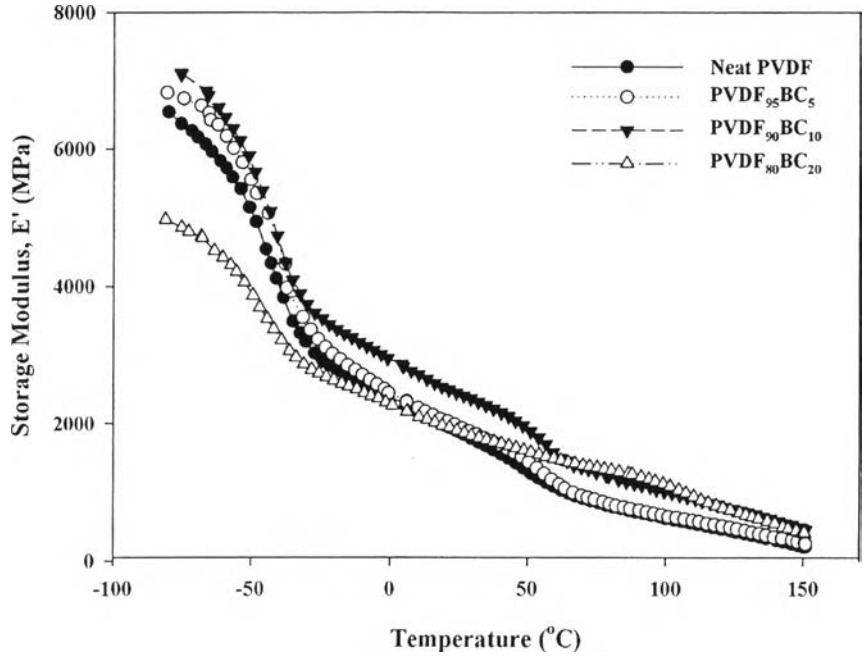

Figure 4.11 Storage tensile modulus, E' vs. temperature of compressed PVDF and 2.5, 5 and 20 wt% BC loading.

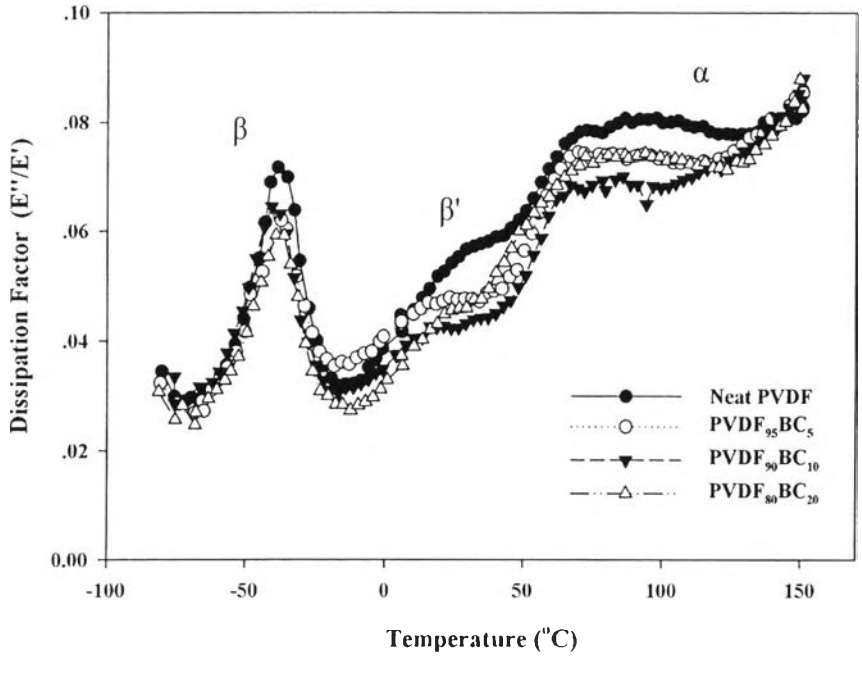

Figure 4.12 Dissipation factor (E''/E') vs. temperature of compressed PVDF and 2.5, 5 and 20 wt% BC loading.

Table 4.5 Summary of transition temperature and storage modulus of PVDF/BC at different composition from DMA technique

Sample	Transition Temperature (°C)			Storage Modulus, E' (MPa)		
	β	β'	α	-50 °C	0 °C	50 °C
PVDF	-38.40	28.83	133.95	5400	2305	1202
$PVDF_{95}BC_5$	-37.70	16.81	122.26	5546	2439	1439
$PVDF_{90}BC_{10}$	-40.60	15.38	128.85	5895	2946	1881
$PVDF_{80}BC_{20}$	-39.00	22.52	107.13	3869	2260	1608

4.4.6 Dielectric Properties of PVDF/BC Blend Films

The dielectric constant related piezoelectric properties, $d_{ij} = \varepsilon_o/g_{ij}$, where d_{ij} is stress piezoelectric coefficient, g_{ij} is strain piezoelectric coefficient and ε_o is the vacuum dielectric constant permittivity (8.85×10^{-12} F/m). Thus, dielectric properties is a basis properties for piezoelectric materials. In this part, the effect of BC content, frequency and temperature on dielectric behavior of PVDF and its nanocomposite were disscussed.

The dielectric properties on temperature dependence of the neat PVDF were shown in Figure 4.13 (a). It was found that the dielectric behaviors of polymer strongly dependent on the variation of frequencies and temperatures, which indicating the presence of relaxation process. According to Hilczer (2002), the glass transition temperature (T_g) of polymer can be determined from dielectric response at low frequency. With increasing in frequency (10 MHz, 100 MHz and 1 GHz), the dielectric relaxation peaks (Figure 4.13 (b)) were shifted to higher temperature (20 °C, 50 °C, and 90 °C) due to a freezing of dipolar motion in the amorphous region.

The variation on dielectric constant of PVDF/BC blend films as a function of temperature (-50°C - 100°C) were shown in Figure 4.14 (a) at frequency of 10 MHz. The enhancing in dielectric constant was found in $PVDF_{90}BC_{10}$ which result from the interfacial polarization between interfaces of both polymers. As the amount of BC reach to 20 wt%, the dielectric constant begins to decrease compare to other compositions. Due to the bubble in the $PVDF_{80}BC_{20}$ films cause lower

interfacial interaction between BC and PVDF as illustrated in Figure 4.4. Figure 4.14 (b) shows the close dissipation factor characteristics of the PVDF/BC blend films. The highest dissipation factor of the blend films at 10 MHz were found at temperature around 20°C.

Figure 4.15 shows dielectric constant (a) and dissipation factor (b) of neat PVDF and PVDF/BC blend films at 2.5, 5, 10 and 20 wt% of BC loading as a function of frequency (10 MHz - 1 GHz) at room temperature. Compared to neat PVDF, blending with 10 wt% BC exhibited higher dielectric constant about 1 over the applied frequency. In contrast, adding BC content up to 20 wt% resulting in decreased dielectric constant as same as temperature dependent (Figure 4.14 (a)). For dissipation factor on frequency dependent, dissipation factor decreases with increasing frequency. However, the combination of BC, the dissipation factor of composite were less than that of neat PVDF through frequency range.

The dielectric constant of compressed composite films as a function of network fiber contents at 20°C are shown in Figure 4.16 (a). The results demonstrated that $PVDF_{90}BC_{10}$ shows higher dielectric constant than neat PVDF and other composites. Moreover, the composite at PVDF/BC weight fraction of 90/10 also shows lower dissipation factor (Figure 4.16 (b)) at 100 MHz and 1 GHz than pure PVDF which refer to the composite has higher potential to stable their dipole moment. Thus, $PVDF_{90}BC_{10}$ composition was chosen to further improving piezoelctric, dielectric and relate properties with basis of piezoelectric touch sensor by loaded MWCNT into composite (disscussed in Chapter 5).

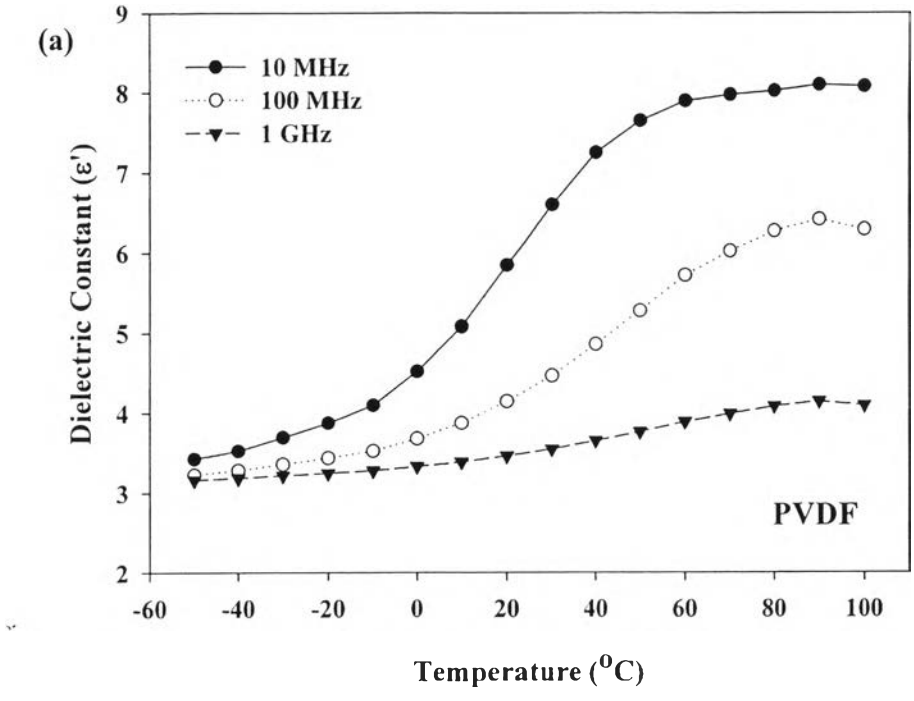

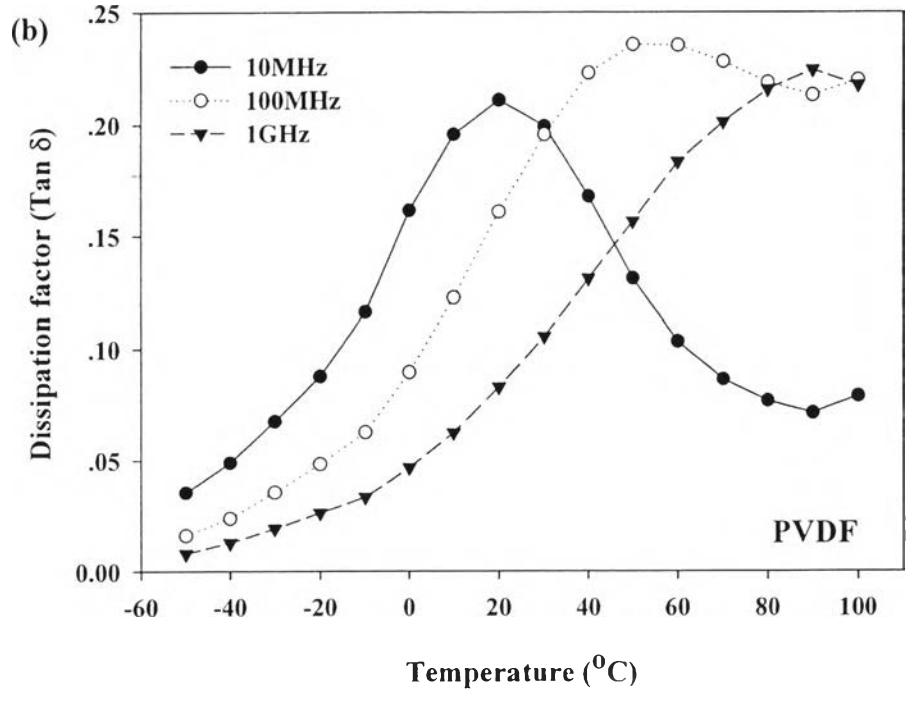

Figure 4.13 Dielectric constant (a) and dissipation factor (b) of neat PVDF film as function of temperature (°C).

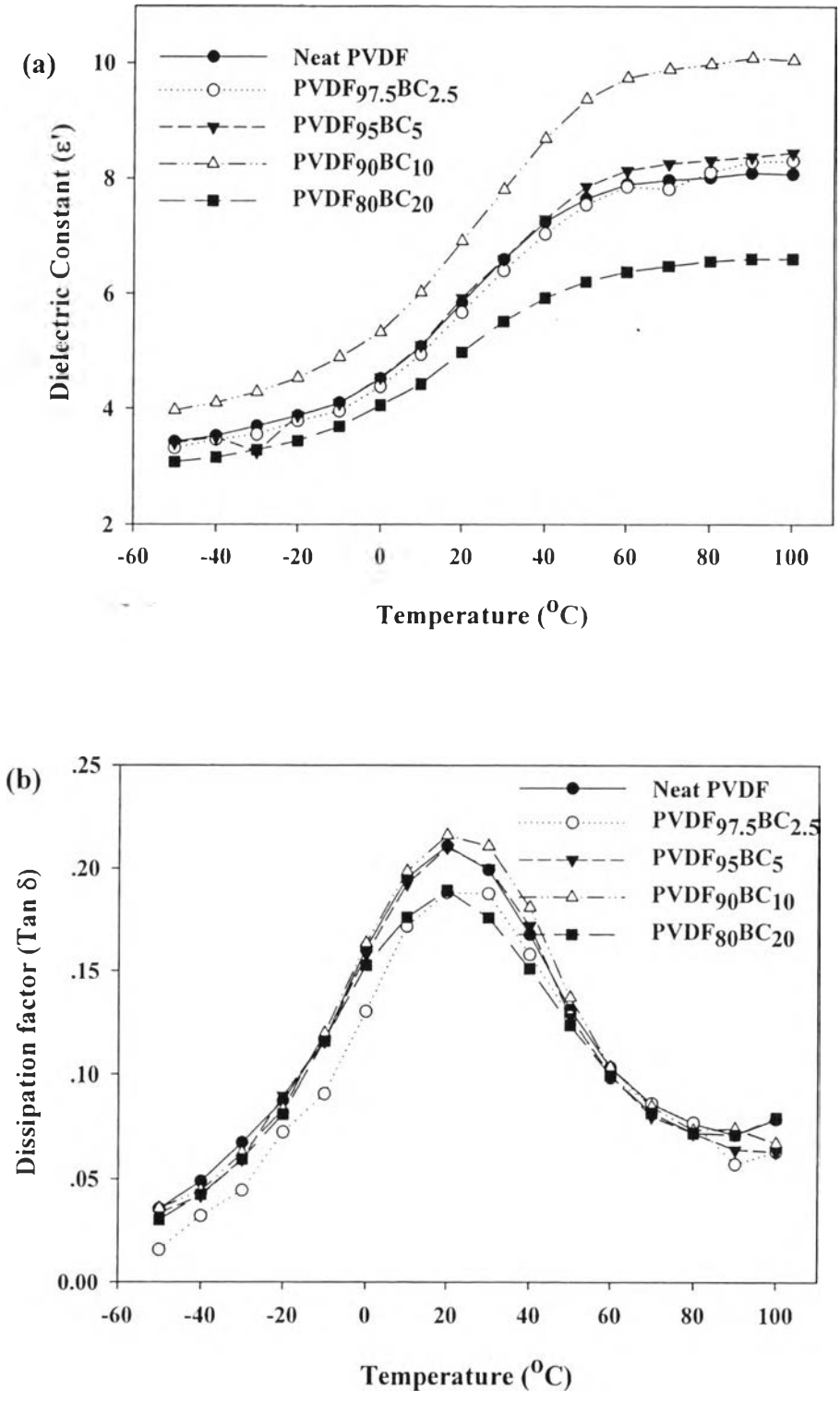

Figure 4.14 Dielectric constant (a) and dissipation factor (b) of PVDF and BC/PVDF blend films at temperature -50°C - 100°C.

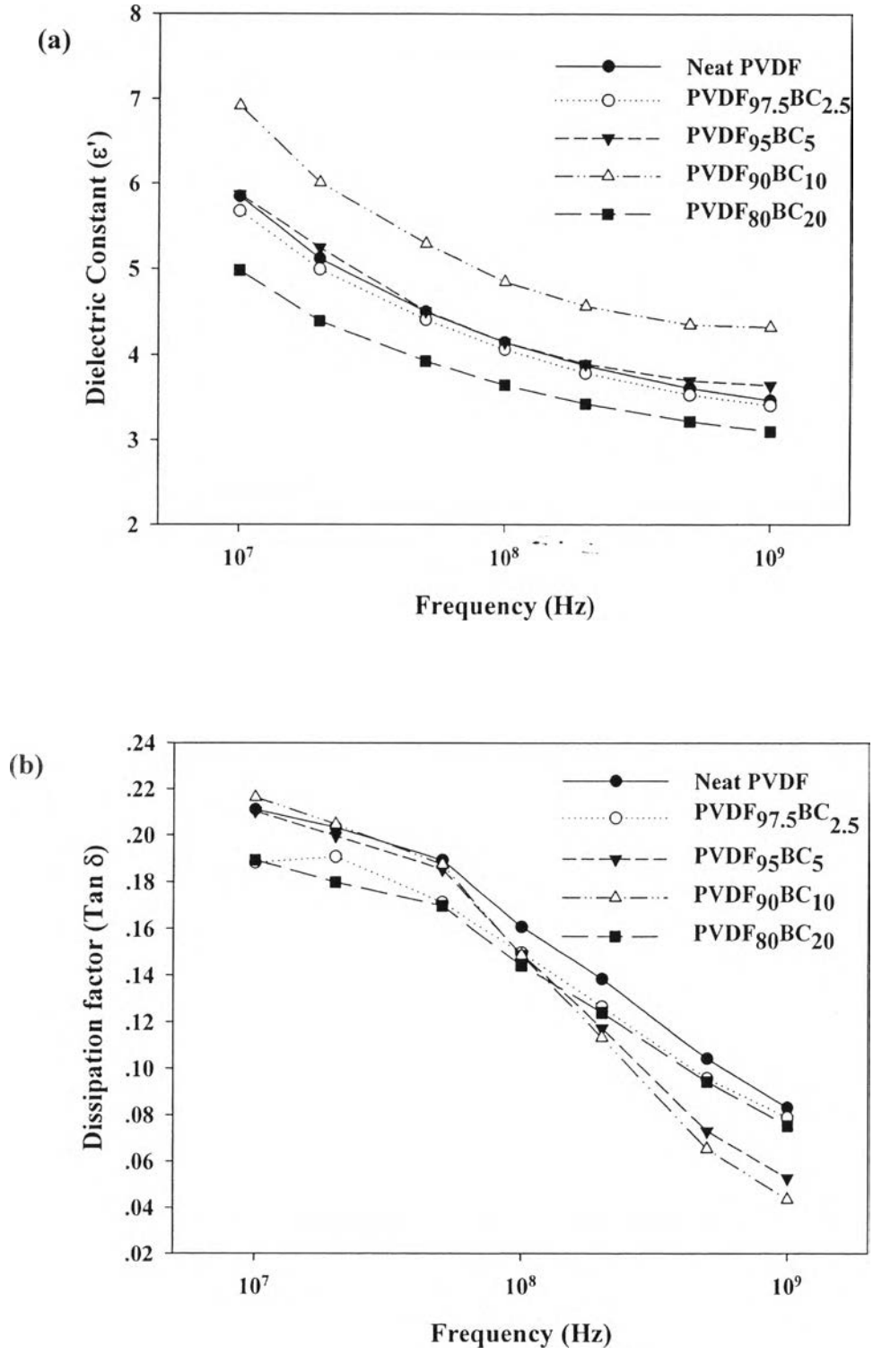

Figure 4.15 Dielectric constant (a) and dissipation factor (b) of PVDF and BC/PVDF blend films as a function of frequency at 20°C.

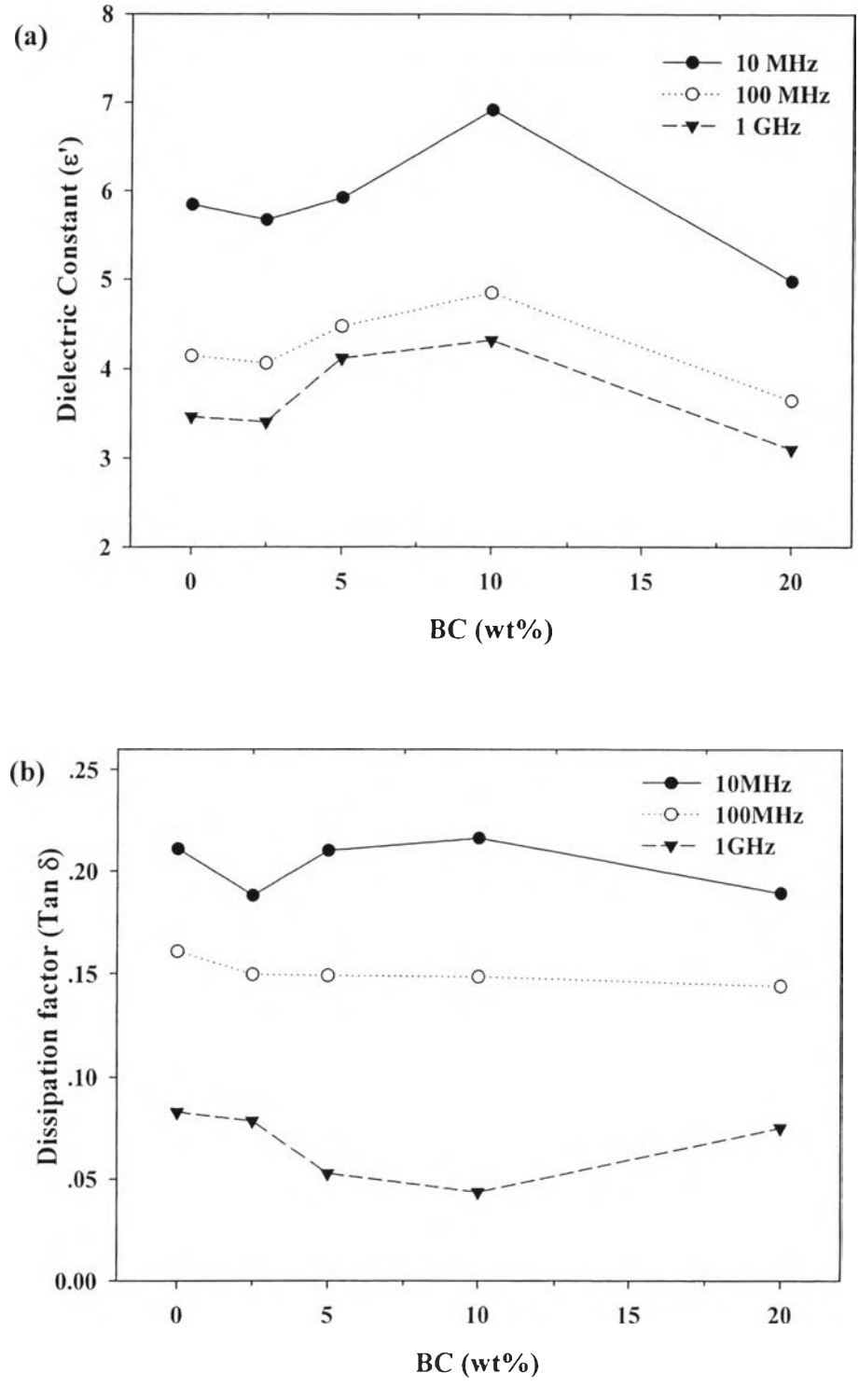

Figure 4.16 Dielectric constant (a) and dissipation factor (b) as a function of BC content for PVDF/BC composite sheets at 10 MHz, 100 MHz, and 1 GHz (20°C).

4.4.7 Ferroelectric Properties of PVDF/BC Blend Films

The piezoelectricity of PVDF has been widely investigated due to the presence of ferroelectric properties. The β cystalline phase of PVDF possesses a highest net dipole moment, molecules are in all trans planar zigzag exhibited lasrgest spontaneous polarization over the other polar polymers. For PVDF/BC blends, this is first studied on ferroelectric properties by observing the hysteresis loop between polarization (P, $\mu C/cm^2$) and electric field (E, kV/cm) as shown in Figure 4.17 and corresponding P-E hyteresis loop are summarized in Table 4.6.

The P-E hysteresis loop of PVDF/BC blends showed small remanent polarization (P_r), almost like that of paraelectric behavior. According to the calculated β-phase content, F(β), from FTIR spectra (Table 4.2), neat PVDF has highest F(β) should exhibited largest polarization but $PVDF_{97.5}BC_{2.5}$ and $PVDF_{90}BC_{10}$ showed higher polarization value. This enhacement in polarization arised from the trapped charged at bacterial cellulose and PVDF interfaces. Fukada (2000) suggested that the charge located in interface are the origin of piezoelectricity and generate piezoelectric phenomena.

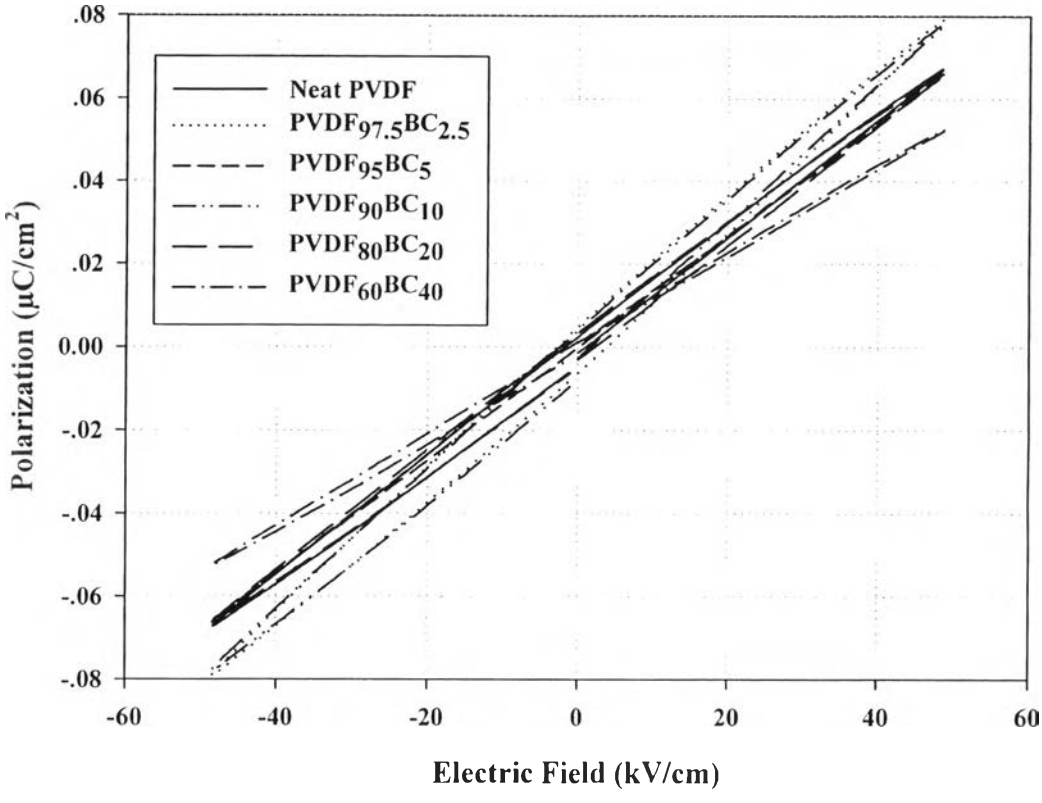

Figure 4.17 P-E hysteresis loop of PVDF/BC blend films at room temperature.

Table 4.6 The polarization profile of PVDF and PVDF/BC blend films

Value	PVDF/BC (wt %)					
	100/0	**97.5/2.5**	**95/5**	**90/10**	**80/20**	**60/40**
P_{Max} (μC/cm²)	0.0671	0.0789	0.0660	0.0778	0.06624	0.05244
P_r (μC/cm²)	0.0024	0.0048	-0.0002	0.0041	0.00342	0.00119
$-P_r$ (μC/cm²)	-0.0064	-0.0086	0.0012	-0.0098	-0.00645	-0.0029
E_c (V/m)	73.6429	233.9358	-92.1962	93.5028	84.2390	0
$-E_c$ (V/m)	-117.436	-176.247	5.3362	-146.95	-91.5324	-52.1359

4.5 Conclusions

Bacterial cellulose (BC) were blended with poly(vinylidene fluoride) (PVDF) by using DMF as a dispersing medium which help to obtain a homogeneously dispersion of nano-fiber in PVDF matrix. The PVDF/BC blend films were prepared using solvent-cast fol86dowed by hot-pressing methods. The SEM micrographs indicated that the BC in casted blend films explored the diameter in nano-scale (about 40-50 nm.) which yield to high surface area and create more intermolecular interaction between oxygen atoms and fluorine atoms. These bio-based nanocomposite films showed the combination of β and α polymorph which had a major form in β piezoelectric phase. The T_g and dynamic T_g of PVDF/BC blends were slightly decreased as increasing BC content. In contrast, the network fiber interrupted the movement of PVDF chain in molten state resulting in enhanced the T_m of nanocomposite films about 1-2 °C higher than that of neat PVDF. The thermal stability of PVDF region in the blend were significantly improved as observed T_d of the blends higher than T_d of neat PVDF about 15-45 °C depend on compositions. The partially interaction between interface of PVDF and BC yield to enhancing both of dielectric and ferroelectric properties at BC 10 wt% loading.

4.6 Acknowledgement

The authors would like to acknowledge the financial support from the National Research Council Thailand (NRCT), grant number GRB_BSS_66_56_63_08 and The Petroleum and Petrochemical College (PPC), Chulalongkorn University.

4.7 References

Adnan, S., Radiah, D., and Biak, A. (2012) The effect of acetylation on the crystallinity of BC/CNTs nanocomposite. Journal of Chemical Technology and Biotechnology, 87, 431-435.

Choi, M.Y., Choi, D., Jin, M.J., Kim, I., Kim, S.H., Choi, J.Y., Lee, S.Y., Kim, J.M., and Kim, S.W. (2009) Mechanically Powered Transparent Flexible Charge-Generating Nanodevices with Piezoelectric ZnO Nanorods. Advanced Materials, 21, 2185–2189.

Czaja, W., Romanovicz, D., and Brown, J.R.M. (2004) Structural investigations of microbial cellulose produced in stationary and agitated culture. Cellulose, 11(3-4), 403-411.

Gregorio, R.Jr. and UENO, E.M. (1999) Effect of crystalline phase, orientation and temperature on the dielectric properties of poly(vinylidene fluoride) (PVDF). Journal of Materials Science, 34(18) 4489 – 4500.

Harrison, J.S. and Ounaies, Z. (2001) Piezoelectric Polymers. 211422 ICASE Report No. 2001-43, National Aeronautics and Space Administration, Langley Research Center, Hampton, Virginia.

Khalil, A., Bhat, A.H., and Yusra, I.A.F. (2012) Green composites from sustainable cellulose nanofibrils: A review. Carbohydrate Polymers, 87, 963-979.

Marcovich, N.E., Auad, M.L., Bellesi, N.E., Nutt, S.R., and Aranguren, M.I. (2006) Cellulose Micro/Nanocrystals Reinforced Polyurethane. Journal of Materials Research, 21(4), 870-881.

Park, W., Kang, M., Kim, H., and Jin, H. (2007) Electrospinning of poly(ethylene oxide) with bacterial cellulose whiskers. Macromolecular Symposia, 249-250(1), 289–294.

Patro, T.U., Mhalgi, M.V., Khakhar, D.V., and Misra, A. (2008) Studies on poly(vinylidene fluoride)–clay nanocomposites: Effect of different clay modifiers. Polymer, 49, 3486-3499.

Ratanakamnuana, U., Atong, D., and Aht-Ong, D. (2012) Cellulose Esters from Waste Cotton Fabric via Conventional and Microwave Heating. Carbohydrate Polymers, 87, 84– 94.

Rao,V., Ashokan, P.V., and Amar, J.V. (2002) Studies on Dielectric Relaxation and Ac Conductivity of Cellulose Acetate Hydrogen Phthalate–Poly (vinyl pyrrolidone) Blend. Journal of Applied Polymer Science, 86, 1702–1708.

Salimi, A. and Yousefi, A.A. (2003) FTIR Studies of β-phase Crystal Formation in Stretched PVDF Films. Polymer Testing, 22, 699–704.

Seydibeyoglu, M.O. and Oksman, K. (2008) Novel Nanocomposites Based on Polyurethane and Micro-fibrillated Cellulose. Composites Science and Technology, 68, 908–914.

Sodsong, T. (2008) Piezoelectric Polymer for Mechanical Sensors in Smart Card Applications. M.S. Thesis, The Petroleum and Petrochemical College, Chulalongkorn University, Bangkok, Thailand.

Tang, C. and Liu, H. (2008) Cellulose nanofiber reinforced poly(vinyl alcohol) composite film with high visible light transmittance. Composites: Part A, 39, 1638–1643.

Uehara, Y., Fukumoto, T., Kamimura, Y., Kuroda, S., Kimura1, T., Date, M., Fukada, E., and Tajitsu, Y. (2011) Piezoelectric Characteristics of Poly(γ-benzyl-L-glutamate) Film Oriented under Strong Magnetic Field. Japanese Journal of Applied Physics, 50(9)